INL/JOU-23-72048-Revision-0

Design and testing of an enriched uranium fueled molten salt irradiation vehicle

October 2023

Abdalla Abou Jaoude, Gregory M Core, Stephen A Warmann, Calvin Myer Downey, SuJong Yoon, Kim B Davies, Bryce James Chandler, Morgan Tess Kropp, William C Phillips, Chuting Tan

Changing the World's Energy Future

Idaho National Laboratory

INL is a U.S. Department of Energy National Laboratory operated by Battelle Energy Alliance, LLC

INL/JOU-23-72048-Revision-0

Design and testing of an enriched uranium fueled molten salt irradiation vehicle

Abdalla Abou Jaoude, Gregory M Core, Stephen A Warmann, Calvin Myer Downey, SuJong Yoon, Kim B Davies, Bryce James Chandler, Morgan Tess Kropp, William C Phillips, Chuting Tan

October 2023

Idaho National Laboratory
Idaho Falls, Idaho 83415

http://www.inl.gov

Prepared for the
U.S. Department of Energy
Under DOE Idaho Operations Office
Contract DE-AC07-05ID14517

Progress in Nuclear Energy 164 (2023) 104846

Contents lists available at ScienceDirect

Progress in Nuclear Energy

journal homepage: www.elsevier.com/locate/pnucene

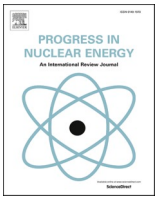

Design and testing of an enriched uranium fueled molten salt irradiation vehicle

Abdalla Abou-Jaoude *, Calvin Downey, SuJong Yoon, Kim Davies, James Chandler, Stephen Warmann, Morgan Kropp, William Phillips, Gregory Core, Chuting Tan

Idaho National Laboratory, Idaho Falls, ID, 83402, USA

ARTICLE INFO

Keywords:
Molten salt reactor
Irradiation
Chloride salt
Fabrication
Testing

ABSTRACT

Molten salt reactors (MSRs) have garnered increasing attention recently with several demonstration efforts on the way. A key challenge to the licensing basis for these reactors is the lack of experimental data on fueled salts. This is expected to be crucial to the safety evaluation and licensing basis of reactors of this type deployed in the future. While capability for irradiating molten salts has been reestablished in the recent decade, no enriched fuel irradiation capability has been developed and tested as of yet. A new experiment vehicle under development at Idaho National Laboratory (INL) is presented here. The Molten-salt Research Temperature-controlled Irradiation (MRTI) experiment was developed to host enriched uranium bearing salt samples to be irradiated at a test reactor within the lab complex. One of the key scientific objectives is to provide irradiated salt samples for post-irradiation examination (PIE) to study the impact of fission product generation and neutron/gamma radioactivity on the salt solution and salt-facing wall material. This paper provides a detailed overview of the mechanical design of the experiment, followed by an overview of the fabrication and assembly of an initial prototype vehicle (with non-fuel-bearing salt). A summary of the key analyses conducted as a part of the performance and safety evaluation is then provided. Lastly, an overview of the test conducted in prototypic out-of-pile (non-neutron) environment are shown. These evaluations provide the foundation for a planned irradiation of an enriched uranium-bearing chloride salt sample in the near term. The upcoming irradiation will contain 13 cm^3 of UCl_3–NaCl salt (93% enrichment) generating around 20 W/cm^3 of fission energy during irradiation and a temperature range that can be contained between bounds of 525–900 °C.

1. Background & introduction

Nuclear energy is a promising candidate for the generation of carbon-free electricity. Several new advanced concepts are being pursued by various global stakeholders both in the private and public spheres. A notable, novel candidate for nuclear energy is the Molten Salt Reactor (MSR). These types of reactors have their fuel dissolved into a salt-based solution. This is advantageous from safety, economic, and waste standpoints. These reactors have passively safe features and do not accumulate fuel irradiation damage in the traditional sense (as is the case with solid fuels). They can operate at low pressure and high temperature, simplifying some of their components and structure. Lastly, certain types of MSRs are intended to re-utilize spent fuel thus drastically minimizing waste generation. These reactors build upon a legacy of two previously operated reactors: the Aircraft Reactor Experiment (ARE) in 1954 (Cottrell et al., 1955), and the Molten Salt Reactor Experiment (MSRE) in 1965 (Thoma, 1971) (see Fig. 20).

However, effective use of these reactors is not without challenges. High temperature salt can be a very corrosive environment for structural material. The accumulation of fission products can drastically alter the chemistry within the salt (e.g., with some of these radioactive products precipitating or bubbling out of the salt). It is therefore crucial to understand the performance of these salt fuels under irradiation. While several of these MSR concepts are being pursued, irradiation capabilities are currently limited.

Several previous irradiation experiments have been conducted in the past as outlined in the overview in reference (Abou-Jaoude et al., 2019). Of notable mention are the natural circulation experiment at the Low Intensity Testing Reactor (LITR) (Savage et al., 1960) and the forced circulation experiment at the Material Test Reactor (MTR) (Trauger and Colin, 1961). Both experiments contained enriched fuel dissolved in a fluoride compound. More recently, several capsule-based experiments

* Corresponding author.
E-mail address: abdalla.aboujaoude@inl.gov (A. Abou-Jaoude).

https://doi.org/10.1016/j.pnucene.2023.104846
Received 5 April 2023; Received in revised form 13 July 2023; Accepted 7 August 2023
Available online 21 August 2023

were conducted at the Massachusetts Institute of Technology Reactor (MITR) (Forsberg et al., 2018) and at the Ohio State University Research Reactor (OSURR) (Ezell et al., 2021). The MITR experiment used a fluoride salt sample while the OSURR sample used chloride salt samples. Both experiments did not contain fissile material. Another recent experiment was conducted at the High Flux Reactor (HFR) in Petten (Hania, 2018). This experiment used fluoride salt samples doped with fertile material (Th).

Several recent efforts have evaluated the design of flowing loops containing enriched salts (Abou-Jaoude et al., 2021a) (Farmer et al., 2022). However, these are considered to be large, very expensive undertakings. As such, recent efforts have focused on a small capsule irradiation of molten salt. The intent is to provide a test vehicle to evaluate the performance of various salt types under irradiation. As a starting point, chloride-based salt candidates were selected for the first demonstration. They were selected as no previous irradiation experiment was conducted using fueled chloride salt. Nevertheless, strong interest in using chloride salts has emerged in industry recently. This is mainly attributed to their higher potential actinide content and better suitability for a fast spectrum configuration (SeY. and Bang, 2016).

2. Experiment design overview

2.1. Experiment requirements and objectives

The irradiation test vehicle is expected to be flexible and provide an ability to irradiate a wide variety of salt samples. However, the current iteration described here has been fine-tuned in order to host fissile material-bearing chloride salt. This type of solution has never before been subjected to a neutron field. The vehicle is also designed to obtain key in-situ performance parameters through the use of instrumentation.

The main objective of the experiment is to produce irradiated samples that can be examined. Post-irradiation examinations (PIE) are expected to revolve around three key objectives. The first is to assess the radiological source term mechanics (namely retention of radionuclides in the salt versus the gaseous plenum or the wall). The second is to study the evolution of thermophysical properties with burnup (primarily due to the accumulation of fission, activation, and corrosion products in solution). The third is to evaluate the impact of irradiation/fission-induced corrosion on materials interfacing directly with the salt.

A final design of this first-of-a-kind experiment is summarized in this article. During earlier design phases (Abou-Jaoude et al., 2021b) (Abou-Jaoude et al., 2021c), a range of parametric analyses were conducted to evaluate different design aspects of the experiment, including the experiment position in the Neutron Radiography reactor (NRAD (Idaho National Laboratory, 2023),) (peripheral or central), facility structural materials of the vehicle, overall dimensions, and ^{235}U enrichment levels. The main design constraints include the temperature limits of the salt-facing material, the allowable reactivity margin in the reactor core, the volume of salt needed for post-irradiation analysis, the salt freezing temperature, and the temperature limits of the reactor coolant-facing material.

Since maximizing fuel burnup also maximizes the possible scientific outcomes of the experiment, it was prioritized over the other technical requirements. Furthermore, a target fission power density of above 20 W/cm^3 while achieving a target average salt temperature of 600 °C was specified as a requirement. This temperature target agrees with MSR design specifications in the literature (Mourogov and Bokov, 2006), (Altahhan and al, 2019). Lastly, the experiment aims to avoid the freezing of salt during reactor operations, due to the risk of radiolysis. This phenomenon could lead to the accumulation of additional gaseous species in the plenum and would impact the plenum source term evaluation during PIE. The chosen binary chloride salt, 33%UCl_3–67%NaCl (mole percent), corresponds to the eutectic composition for the compound, maximizing the allowable temperature range for the experiment.

The main design challenge regarding the experiment stems from the competing objectives of enabling fission heat dissipation during neutron irradiation, while simultaneously limiting heat loss during startup, prior to the beginning and end of reactor operations (in order to keep the salt molten while reactor gamma rays are being emitted). As a result, an immersion heater design was chosen over a furnace-type approach in order to satisfy both requirements. The resistive heater is placed within a thermowell and controls the temperature of the experiment (regardless of whether the reactor is on or off). A gas gap between a double walled containment can have a fine-tuned mixture of gases to control heat losses based on experiment needs (this is particularly useful if future iterations of this experiments consider other types of salt).

A secondary objective of the experiment is to test instrumentation in a high temperature, salt-interfacing irradiation environment. Four instrumentation positions exist in the Molten-salt Research Temperature-controlled Irradiation (MRTI) test vehicle. Two will be contained within thermowells to avoid direct contact with the salt. One of the sensors is expected to be a thermocouple (TC) that will monitor the salt temperature. Other possible instruments under consideration include neutron detectors, needle probes, pressure gauges, and electrochemical sensors (McDuffee et al., 2022).

At least 5 mL of fuel-bearing chloride salt must be recovered for post-irradiation examination (PIE) to perform the analyses necessary to achieve the experimental objectives. The host reactor for the experiment is the Neutron Radiography (NRAD) facility at Idaho National Laboratory (INL). This is a so-called 'Training Research Isotope General Atomics (TRIGA)' reactor that is water cooled with an array of highly enriched uranium (HEU) fuel elements. The experiment will be placed within an assembly that mimics an existing NRAD three-pin cluster, with the fourth pin used for the experiment, and inserted into the F1 position in the reactor as shown in Fig. 1. It will have an open-top fitting so instrumentation cables can be connected to the control system outside the NRAD reactor.

In the longer term, the experiment is expected to be led to follow-on irradiations with various possible combinations of fueled salt and wall

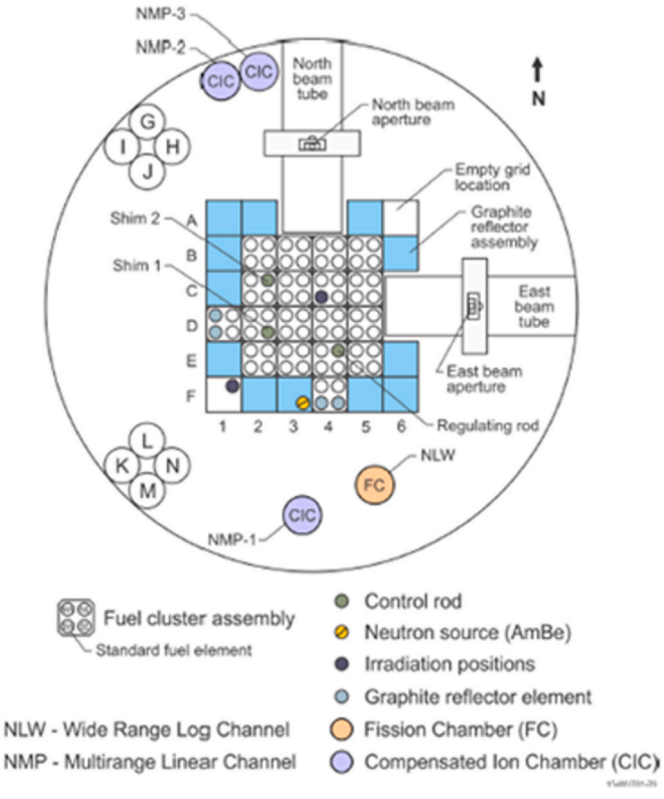

Fig. 1. NRAD core configuration and layout (from (Bess et al., 2014)).

material. Further into the future, this experiment is expected to prove to be a steppingstone for larger experiments with circulating fueled salt in the Advanced Test Reactor (ATR) (Abou-Jaoude et al., 2020).

2.2. Salt-bearing capsule overview

Functional and operational requirements drove design requirements for the salt-bearing capsule, where material choice of the capsule is one of the first critical design considerations, encompassing factors including neutronics contributions, operational temperature, structural strength, and corrosion performance, as well as fabricability and material supply chain. With these considerations, the capsule materials under consideration were Inconel 625 (IN625), Inconel 617 (IN617), and stainless steel 316/316 L (SS316) for their high strength, corrosion resistance, and ample supply chain. Both IN625 and IN617 show improved strength at the high operational temperatures involved in the experiment in comparison to SS316. Neutronics comparisons between the three materials indicated that IN625 results in the lower neutron absorption and thus lower negative reactivity contribution to the system in comparison to IN617. An additional consideration in the design was the inclusion of tantalum (Ta) versus niobium (Nb) in the IN625, as Ta has a higher absorption cross-section in the thermal neutron spectrum. Ultimately IN625 with minimal Ta content was chosen as the desired material for the salt-bearing capsules. In the interest of corrosion analysis in PIE, IN625 was designed to be the only material in contact with the salt to avoid any galvanic corrosion effects (i.e., no dissimilar salt-facing material).

Due to the packing factor of synthesized salt powder (~60%), the inner capsule internal volume was designed to account for the volume decrease of salt when melted, as shown in Fig. 2 Component 8. Therefore, a plentiful plenum space would be contained in the capsule where fission gas and chloride gas would collect. With this plenum design, the pressures and stored energy involved in system (Section 3.3) during operation were low enough to allow for thin-walled capsule geometry (0.028 inches (0.71 cm) or less), shown in Fig. 2 Component 1. This allows for laser-based gas extraction PIE techniques described in later sections. The diametral geometry of the capsule is largely a factor of heater style and design, as well as external interface requirements with typical NRAD reactor core assemblies discussed in later design considerations. This capsule will be sealed via assembly procedures involving brazing and plug welding (See Fig. 2, Item 7). Upon sealing the capsule assembly, a pure argon atmosphere is filled within the capsule planum (Fig. 2, Item 6).

Though external furnace designs have been used in the past for irradiated molten salt experiments, these designs are unable to incorporate high fuel enrichments with appreciable fission power due to a lack of sufficient heat transfer out of the salt-bearing capsule once it is self-heating. For this reason, an axial immersion heater is a crucial design choice for these fuel-bearing salt irradiation experiments. Therefore, an 800 W Watlow immersion heater was specified to be used to melt the powder salt in the reactor position prior to irradiation and to provide supplemental heat input during the experiment (Fig. 2, Item 5). This heater features an integrated Type K thermocouple to serve as the overtemperature shut-off sensor. The designed heated section of the heater will be the bottom 3 inches (7.62 cm) of the capsule where the molten salt will reside below the plenum. Because the heater sheath is Incoloy 800 (GmbH, 2023), the heater will be placed inside of a thin wall thermowell made of IN625 as seen in Fig. 2, Item 2. This heater is designed with a 0.375 inch outer sheath diameter and the thermowell is designed with a 0.030 inch (0.076 cm) thickness, resulting in a total diameter of 0.435 inches (1.105 cm). Thus, both the salt annulus thickness and capsule diameter must be designed around this inner diameter. To achieve a total salt volume of greater than 14 mL and with PIE mockup activities, a salt annulus thickness of 0.4 cm was chosen (Fig. 2, Item 8).

In order to control the temperature of the salt prior to irradiation with heater power input and during irradiation with fission heat, the radial thermal conductivity to the NRAD coolant is controlled via an inert gas gap. This gas gap thickness and concentration (mix of inert gases such as helium, argon, and xenon) ultimately controls heat transfer from the capsule and is sized based on thermohydraulic analysis discussed in further sections. Based on iterative thermal analysis the gas gap thickness was identified to be nominally 0.030 inches (0.076 cm) and a mix of 85% argon and 15% helium. The gas gap thickness is held

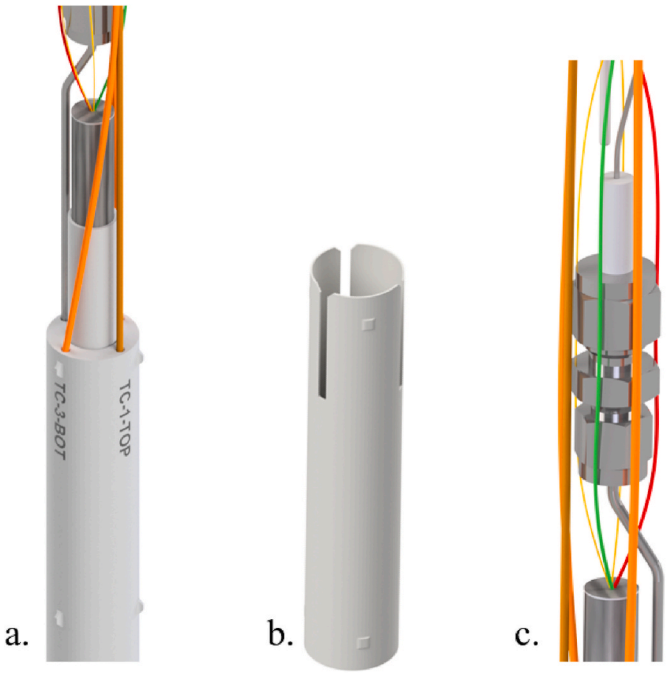

Fig. 3. Shows aspects of MRTI capsule design. a) Capsule gas ga standoff geometries, b) Radiative heat shield, and c) Optical fiber pressure sensor and Swagelok connection.

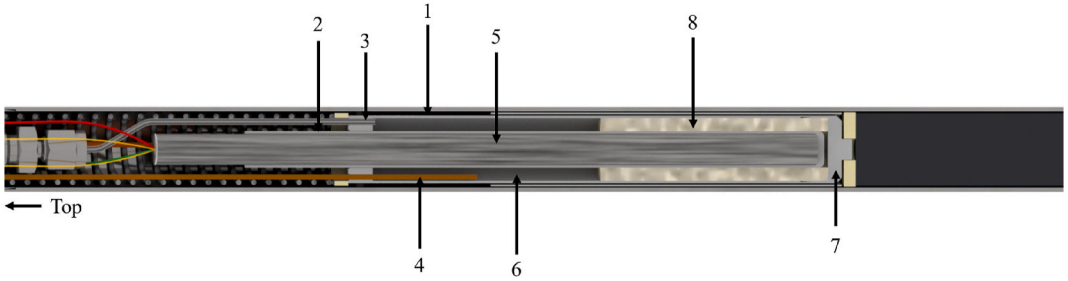

Fig. 2. Half section view of MRTI capsule design. 1.) Capsule, 2.) Capsule heater thermowell, 3.) Pressure tube extension, 4.) Type-N thermocouple, 5.) Immersion heater, 6.) Plenum, argon gas, 7.) Capsule plug, 8.) Molten salt volume.

via standoff geometries machined on the outer diameter of the capsule as shown in Fig. 3a. These standoff geometries hold the nominal gas gap against the inner diameter of the capsule containment. Further thermal analysis revealed that high temperatures in the experiment drive heat loss via radiative heat transfer. Therefore, a radiative heat shield was designed in order to reduce radiative heat loss directly into the capsule containment and into the NRAD coolant water (Fig. 3b). This component is machined out of SS316L and is centered between the capsule and the outer containment inner diameter via similar standoff geometries.

Multiple Type-N IN625-sheathed thermocouples (Fig. 2 Item 4) will be placed at varying axial positions to provide continuous data on the average temperature in the salt. Type N thermocouples were chosen for superior radiation resistance in comparison to Type K thermocouples over prolonged exposure to neutron irradiation. Changes in plenum pressure will be monitored via an optical fiber pressure sensor assembly fabricated at INL's Measurement Sciences Laboratory (MSL) (Fig. 3c). This pressure sensor will be connected into the capsule via an extension tube due to size constraints involved in direct connection (Fig. 2, Item 3). The pressure sensor will be sealed onto this extension tube via a Swagelok compression union fitting. This pressure measurement system will not provide data on exact plenum pressure within free volume but will inform changes in pressure as a function of burnup of the molten salt. The heater thermowell, thermocouples, and pressure sensor will be induction brazed through the top of the inner capsule.

2.3. Experiment vehicle assembly

The MRTI inner capsule is assembled in an outer can containment which ultimately seals the experiment from the NRAD coolant water and maintains the gas gap composition of the experiment (Fig. 3, Item 1). This outer can containment is machined out of SS316L and is designed for the outer diameter of NRAD fuel elements (1.022 inches [2.596 cm]) to maintain prototypic cooling conditions as is present on adjacent fuel clusters. Total radial dimensions of the MRTI capsule and outer can containment are listed in Table 1.

In order to maximize the heat generation rate of the molten salt, the midplane of salt will be placed at NRAD fuel midplane via a graphite bottom spacer. Graphite was chosen as the spacer to maintain as much moderating material in the experiment as possible to compensate for water displacement (taken up by the experiment). High purity (nuclear grade or similar) was specified for graphite material to reduce potential boron and ash impurities. Between the capsule and the bottom graphite moderator an insulative spacer will minimize axial heat transfer out of the bottom of the inner capsule (Fig. 4, Item 4). The material for the insulative spacer was specified to be bisque-fired alumina material (AREMCO, 2023). The geometry of the spacer includes axial struts as to maintain a gas gap under the inner capsule cap. Internal components including the capsule, insulative spacer, and graphite spacer, are held axially static by a SS302 compression spring in the assembly (Fig. 4, Item 6). To reduce the potential of heat transfer into the compression springs and loss of elasticity, a similar insulative spacer is placed between the top of the inner capsule and the compression springs. This insulative spacer is designed with an annular geometry in order to allow routing of instrumentation through it into the upper section of the outer can containment. The top of the outer can containment increases in diameter to 1.5 inches (3.81 cm) to interface with existing NRAD fuel cluster hardware. This is achieved via a welded top can fitting component (Fig. 4, Item 3), and this component also provides the shoulder for the compression springs in the assembly. Instrumentation and heater leads are routed around the Swagelok fitting (Fig. 4, Item 7) and through the upper section of the outer can containment and inserted through a Conax compression seal fitting at the top of the assembly (Fig. 4, Item 9). Because heater leads in the experiment are not Mineral Insulated Cable (MIC), a custom potting cup transitions this cabling to water-proof cabling, and the compression seal seals onto the outer diameter of this potting cup (Fig. 4, Item 8). Compression seal internals were specified to be Grafoil material in order to reduce gas leakage from the outer can containment, in comparison to other seal options such as Teflon or Lava. The MRTI experiment assembly is backfilled through this Conax during assembly with the identified gas gap composition.

Table 1
MRTI component radial dimensions.

Component	Material	Diameter (cm)
Immersion Heater	Incoloy-800 Sheath	0.94
Heater Thermowell	IN625	1.10
Salt Annulus OD	0.33UCl3-0.67NaCl	1.90
Capsule OD	IN625	2.04
Radiative Heat Shield ID	SS316L	2.13
Radiative Heat Shield OD	SS316L	2.23
Outer Can ID	SS316L	2.31
Outer Can OD	SS316L	2.60

The MRTI experiment vehicle is installed in a typical NRAD cluster assembly for reactor installation (Fig. 4, Item 4). Because the cluster assembly requires a total of four pins for assembly, three dummy aluminum pins are used to act as the fuel pins in this cluster. Additional fuel pins and graphite-filled pins were in this cluster assembly design but may affect neutronic performance of the system. Other salt experiment pins and materials may be considered for these three additional pin positions in the cluster. The pins and the MRTI experiment vehicle are installed in the bottom cluster end fitting (Fig. 5, Item 3).

2.4. Instrumentation and controls

The temperature control system for the MRTI experiment is based around an Allen- Bradley 5069-L306ER Programmable Logic Controller (PLC) with a micro 820 used for subsidiary inputs. Dual zone heat control allows another similar experiment to be run in the reactor at the same time. The PLC will be located in the hallway to the north of the cask transfer tunnel, a short distance west of the reactor room, with instrumentation run through the wall into the cask tunnel and along the cask tunnel wall through a narrow portion of the lead shielding wall of the reactor room that will not interfere with door operation. Additional shielding is placed in front of the feedthrough area sufficient to allow for similar or better streamed radiation shielding than the original wall. Thermocouple extension leads and the heater power cables then go down into the reactor tank and the watertight Conax seal at the top of the experiment capsule. Separate wiring is provided from the control panel into the reactor control room to allow for a direct electrical disabling of both heaters independently from the main reactor control bench and a Human Machine Interface (HMI) running on a touchscreen computer near the operator as they sit at the bench. This experiment is integrated into a larger suite of experiment control systems accessible through the same HMI and can be run in the background for long term irradiation experiments or as other events go on in the reactor. All data from the experiment instrumentation and the reactor control system is logged and can be accessed to inform expected outcomes or PIE interpretation.

Instrumentation in the capsule itself consists of three type N thermocouples placed at equal radial distances in the experiment capsule and a 90-degree separation. Each is also at a different height relative to the Conax seal. At the fourth perpendicular location is a fiber optic pressure sensor. A self-powered neutron detector and a type K thermocouple at the heater finish out the instrumentation package in the experiment. All four thermocouples are connected to signal conditioners at the control panel outputting in voltage, allowing the signals to be shared from both the main PLC and a completely independent overtemperature controller. Any thermocouple signal can therefore be switched into the overtemperature circuit, and all are always fed to the PLC for data recording. This allows the continued operation of the heater in the experiment in the event that any thermocouple or thermocouple lead becomes damaged and no longer provides a signal. The switching

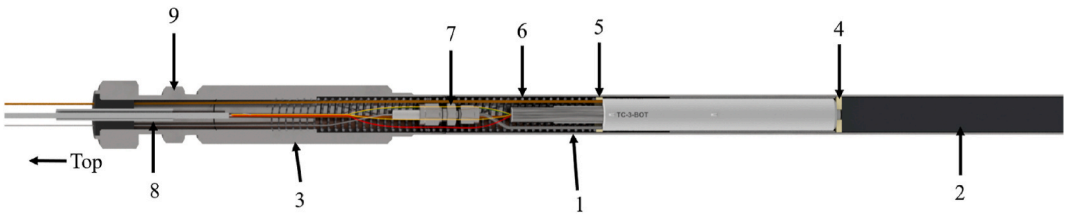

Fig. 4. Cross-section view of the MRTI outer can containment design. 1.) Outer can geometry, 2.) Graphite spacer, 3.) Outer can top fitting, 4.) Bottom insulation spacer, 5.) Top insulation spacer, 6.) Compression springs, 7.) Swagelok fitting, 8.) Leadout potting cup, and 9.) Top compression seal fitting.

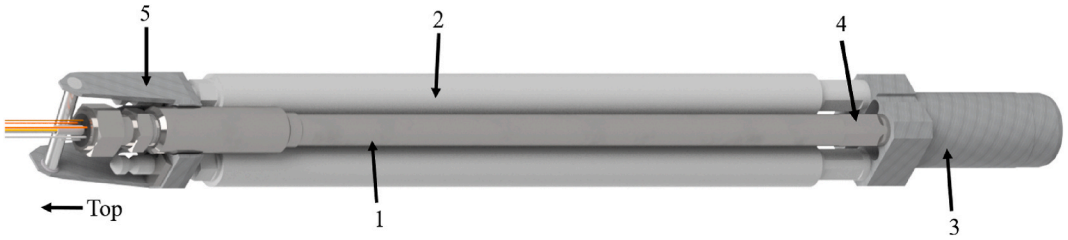

Fig. 5. Isometric view of the MRTI cluster design. 1.) MRTI experiment vehicle, 2.) Aluminum pins, 3.) Bottom cluster end fitting, 4.) MRTI bottom fitting, 5.) Top cluster bail.

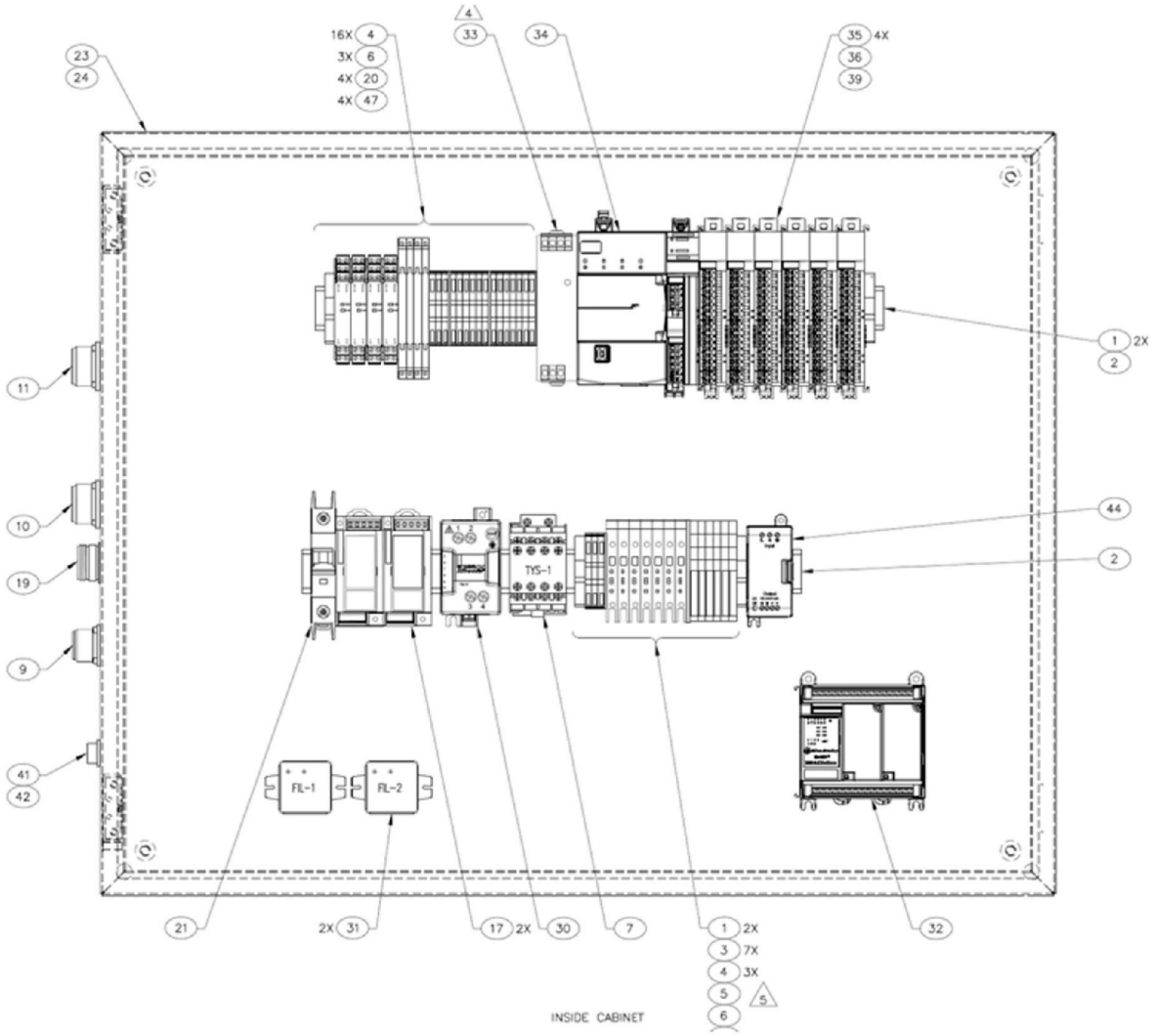

Fig. 6. Overview of the controller drawings for controlling the experiment temperature.

itself is accomplished through the PLC, but there is always at least one thermocouple signal present, preserving the independence of the over-temperature controller.

The heater control is tuned by an advanced Proportional-Integral-Derivative (PID) tuning algorithm developed by Rockwell enabling precise heater control, which coupled with the cooling water present in the reactor will allow for good overall temperature control. Expected thermal use of the reactor coolant is low and will be verified to be within operational requirements specified by reactor personnel in a commissioning test prior to the experiment being placed into the reactor. The control system will maintain the experiment temperature in the molten salt range while the reactor starts up or shuts down. Minimal heating is expected to be required while self-heating is active. The shut-down temperature for this experiment is set to 1100 °C. An overview of the control system drawing is shown in Fig. 6.

2.5. Salt synthesis

The fuel salt for the in-pile experiment was synthesized at the INL Materials and Fuels Complex in the custom designed argon atmosphere Class B radiological pyrochemistry glovebox (MBraun, Fig. 7), which was maintained at less than 5 ppm O_2 and 2 ppm H_2O. Balances (Mettler-Toledo) used for preparation of the salt were calibrated by the INL calibrations and standards laboratory and assigned an uncertainty of ± 0.10 g, with a readability of 0.01 g. Daily balance checks were performed with calibrated check weights prior to operations to ensure that measured weights were accurate within the stated uncertainty band. Feedstock uranium metal was legacy material from the Zero Power Physics Reactor that was enriched in U-235 to 93.17%. The sodium chloride was anhydrous 99.99% purity procured from Alfa-Aesar and was further dried by baking at 350 °C under rough vacuum for 24 h. Further details of the fuel salt synthesis are proprietary; however, the resulting fuel salt is composed of the NaCl–UCl_3 binary eutectic at 33.3 mol% UCl_3 and 66.7 mol% NaCl. The resulting ingot of fuel salt is shown in Fig. 8. Samples are to be sent to the INL Analytical Laboratory for trace element analysis and confirmation of bulk composition prior to in-pile operations. Previous analysis of salt synthesized using the same process with depleted uranium feedstock has shown purity levels of 99.98% or greater, with the uranium concentration within ± 0.5 mol% of the target value.

3. Experiment performance analysis

This section discusses initial calculations conducted in order to predict the experiment behavior while in the reactor. The main purpose is to identify key performance parameters and ensure the experiment can operate within safety bounds. This section will first outline the neutron transport simulations that were used to obtain heating rates in the experiment among other things. These were then fed to thermal hydraulic models to predict temperature ranges and heater power levels. Lastly, some discussion of the anticipated stresses in the experiment are provided.

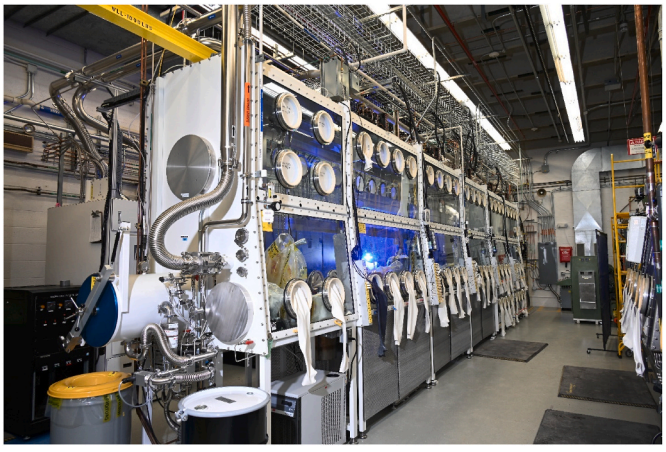

Fig. 7. Pyrochemistry glovebox in the Fuels and Applied Science Building at the Materials and Fuels Complex.

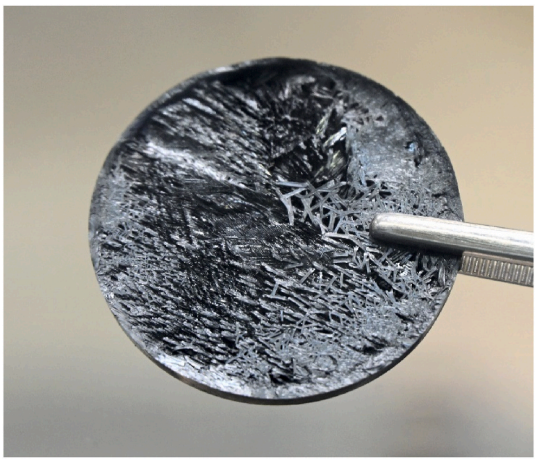

Fig. 8. Synthesized NaCl–UCl_3 eutectic salt ingot to be used in the MRTI in-pile experiment vehicle.

3.1. Neutron transport simulations

The neutron transport code MCNP6.1 (Monte Carlo Neutral Particle) was used for the neutronic analysis (Pelowitz et al., 2013). A representative model of the NRAD core geometry was used for this purpose, with the experiment explicitly modeled within the core geometry, as shown in Fig. 9. A total of 200,000 virtual particles were simulated by the code over 800 cycles (700 active). This represented 1.6 E+8 particles and led to a satisfactory standard deviation in the eigenvalue of 0.00007, and a stochastic uncertainty of 0.31% on the salt heat generation (an important metric for the analysis). Both neutrons and photons are accounted for in the simulation.

The salt sample selected for the experiment is 0.33UCl3-0.67NaCl. A feed of HEU was identified, and the corresponding U-vector is detailed in Table 2. HEU vector composition and mass used in the MRTI salt sample. The correlation for the salt density was obtained from (Desyatnik et al., 1975) and is shown below.

$$\rho(T) = 3.8604 - 8.37 \times 10^{-4} \times T$$

A temperature of 600 °C was assumed for estimating the salt density. Note that this is slightly below the temperature range quoted in (Desyatnik et al., 1975) but it is still considered to be a useful approximation. The resulting salt composition is summarized in Table 3. Estimated salt sample characteristics in MRTI experiment. All other materials used in the experiment (e.g., MgO, IN-625, SS-316, Ar, Cu, Ni, graphite, etc.) are all typical 'off-the-shelf' materials.

The overall reactivity impact of the experiment on the core was estimated by comparing the eigenvalue in the model against a 'base' model using the relation:

$$\Delta\rho(\text{pcm}) = \frac{k_{MRTI} - k_{base}}{k_{MRTI} \times k_{base}} \times 10^5$$

$$\Delta\rho(cents) = \frac{\Delta\rho(\text{pcm})}{\beta} \times 100$$

Here, $\Delta\rho$ represents the change in reactivity (k) and β is the delayed neutron fraction in the core. The value estimated by MCNP was 0.0078. To ensure an 'equivalent' comparison, the base case leveraged the MRTI

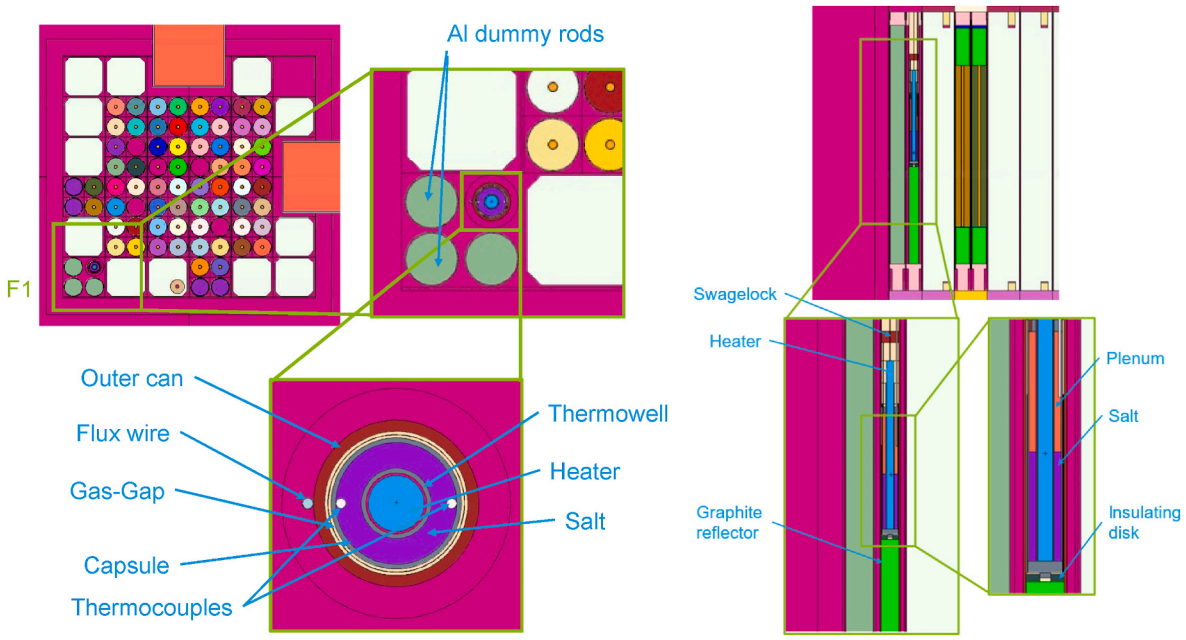

Fig. 9. Visualization of the MCNP-generated geometry for the reactor with experiment. Cross-sectional view of the MRTI experiment in the XY plane (left) and YZ plane (right).

Table 2
HEU vector composition and mass used in the MRTI salt sample.

	^{232}U	^{234}U	^{235}U	^{236}U	^{238}U
Weight Fraction	0.0%	1.0%	93.2%	0.3%	5.6%
Mass (g)	3.771E-06	0.206	19.522	0.057	1.166

Table 3
Estimated salt sample characteristics in MRTI experiment.

Parameter	Value
Salt density	3.13 g/cc
Salt volume	13.05 cc
Salt mass	40.85 g
U mass in salt	20.95 g
^{235}U mass in salt	19.52 g
Na mass in salt	4.10 g
Cl mass in salt	15.08 g

Table 4
Estimated heat generation rates in different regions of MRTI.

Component	Volume (cc)	Total Power (W)	Power Density (W/cc)
MRTI Salt Sample	13.05	253.08	19.39
Capsule Radial	6.28	1.51	0.24
Heater Thermowell	4.42	0.92	0.22
Bottom + Slot	1.52	0.40	0.26
Capsule top	1.69	0.28	0.17
Outer Shell	68.93	8.67	0.13
Hot TC	0.58	0.05	0.08
Plenum TC	0.49	0.03	0.07
Cold TC	0.69	0.07	0.10
Pressure tube	0.12	0.01	0.11
Cu	0.07	0.00	0.07
Bottom Graphite Reflector	102.05	2.32	0.02
Lower Insulator disk	1.37	0.07	0.05
Upper Insulator disk	0.44	0.01	0.03
Spring	0.47	0.03	0.07
Swagelok	5.40	0.02	0.004
Heat Shield	4.59	0.98	0.21

experiment and converted all the materials in the experiment to water to mimic an empty F1 position.

The resulting reactivity impact of MRTI was calculated to be 0.01 ± 1.07 ¢. Since the standard deviation is larger than the actual reactivity, the impact of the experiment on the eigenvalue is essentially negligible. The variation is essentially not even statistically significant. As a result, this is well within the 45 ¢ NRAD limit to ensure the reactor will not be xenon-precluded under equilibrium xenon conditions.

Heat generation rates in the MRTI experiment are summarized in Table 4. The heating rates were provided to guide the thermal analysis of the experiment. The vast majority of heat is generated directly within the salt, as expected. When evaluating the fission heat generated by the salt (using an F7 tally), a value of 20.52 W/cc was obtained. This is higher than the 19.39 W/cc value reported in Table 4 as it does not account for gamma-based energy deposition outside the salt boundary. Nevertheless, the 20 W/cc programmatic requirement relates to burnup and therefore fission heat in the experiment.

To provide additional granularity, a mesh tally was employed to evaluate spatial self-shielding effects in the salt. The salt annulus is radially split (R) in two parts, axially (Z) split in three sections, and azimuthally (Th) divided into four quadrants. The results are shown in Table 5. The hottest point in the salt corresponds to the quadrants facing the NRAD core, at the section closest to the capsule wall and at the axial height closest to the center of the NRAD fuel. The averaged heat generation rates agree to within 3.5% with the value quoted in Table 4. The peak/average ratio in heat generation is 1.486. These various heat generation rates were fed into the analysis of Section III.B.

3.2. Thermal hydraulics simulation

The central heater creates a radial temperature gradient in the salt leading to natural convection. The natural convection of salt will reduce the difference between the maximum and minimum salt temperature by the salt mixing and the convective heat transfer. The salt near the heater flows upward due to the buoyancy effect then flows downward near the inner wall of the capsule. The heat is conducted through the capsule wall and then radiated to the outer wall by the radiation heat transfer in the

Table 5
Mesh tally result showing heat generation distribution within the salt. The radial and axial values are in (cm) while azimuthal ones are in revolution.

R	Z	Th	W/cc
0.65	1.167	0.125	17.96
0.65	1.167	0.375	16.22
0.65	1.167	0.625	14.84
0.65	1.167	0.875	16.13
0.65	3.500	0.125	14.59
0.65	3.500	0.375	13.30
0.65	3.500	0.625	11.67
0.65	3.500	0.875	13.13
0.65	5.833	0.125	17.11
0.65	5.833	0.375	16.17
0.65	5.833	0.625	14.41
0.65	5.833	0.875	15.53
0.85	1.167	0.125	27.79
0.85	1.167	0.375	24.38
0.85	1.167	0.625	20.01
0.85	1.167	0.875	24.16
0.85	3.500	0.125	24.31
0.85	3.500	0.375	20.50
0.85	3.500	0.625	16.53
0.85	3.500	0.875	21.02
0.85	5.833	0.125	25.66
0.85	5.833	0.375	22.12
0.85	5.833	0.625	18.84
0.85	5.833	0.875	22.58

gas gap between the capsule and outer wall. The thermal radiation shield reduces the radiation heat transfer from the capsule to outer wall and environment.

The conjugate heat transfer analysis with radiation heat transfer model was performed to evaluate the temperature distribution in the MRTI experiment capsule, taking into account the physics aforementioned. The natural convection of the salt in the capsule was solved by adopting Reynolds-Averaged Navier-Stokes (RANS) equation-based segregated flow and segregated fluid temperature solvers, the gravity model, and Shear Stress Transport (SST) k-w turbulence model with all y + wall treatment model. For gas regions (cover gas and gas gap), the surface-to-surface radiation (S2S) model with gray thermal radiation spectrum model was employed. To ensure accurate heat transfer analysis, temperature-dependent material properties were employed for each component (NIST Chemistry Webbook, 2023);Special Metals, 2023; Silfka et al., 1998. However, in the case of the salt, the thermal conductivity remains uncertain, and only upper and lower bounds were available for analysis. To investigate the effect of this uncertainty, Computational Fluid Dynamic (CFD) simulations were conducted using both the maximum (0.5 W/m-K) and minimum (0.2 W/m-K) thermal conductivities of the salt. The emissivity of the stainless steel was assumed to be 0.3 (ASM International, 1990). The emissivity of the Inconel-625 was set to be 0.16 (Kieruj et al., 2016). The heat transfer through solid regions was solved by the segregated solid energy solver. The MRTI device is cooled by the water flow outside the outer wall. The ambient temperature of 40 °C and the convective heat transfer coefficient were specified on the outer wall boundary to account for the external convective heat transfer as follows:

$$h_{wall}\left[\frac{W}{m^2K}\right] = -1.4269\times10^{-2}\bullet T^2 + 17.933\bullet T - 2636.5 \quad (313.15\ K \le T \le 422.817\ K)$$

The heat loss through the insulation wafer may decrease the minimum salt temperature and result in the freezing of the salt at the bottom of the device. To ensure a conservative analysis, the heat loss through the insulation wafer was assumed to be approximately 3.5–4.6% of total heating power.

Fig. 10 illustrates the computational mesh structure of the CFD model. The computational mesh was generated using the unstructured polyhedral mesh with the prism boundary layer mesh for the near-wall mesh refinement. The total number of prism boundary layers is four. The base sizes of the mesh for fluid domains and solid domains are 0.2 mm and 1.0 mm, respectively. These mesh parameters were determined based on the mesh sensitivity test.

3.2.1. CFD results for fission-off test

Various heater powers were tested to investigate the experimental feasibility. In this test, no fission heating is assumed, and only the heater provides the thermal energy to the device. Fig. 11 shows the temperature distribution of the MRTI device. When the thermal conductivity of the salt was 0.2 W/m-K, the highest heater volumetric heat generation rate of 80 MW/m^3 resulted in a salt temperature too high (1622.82 °C) that is far from the valid property ranges (868.85 °C) of the salt. In this

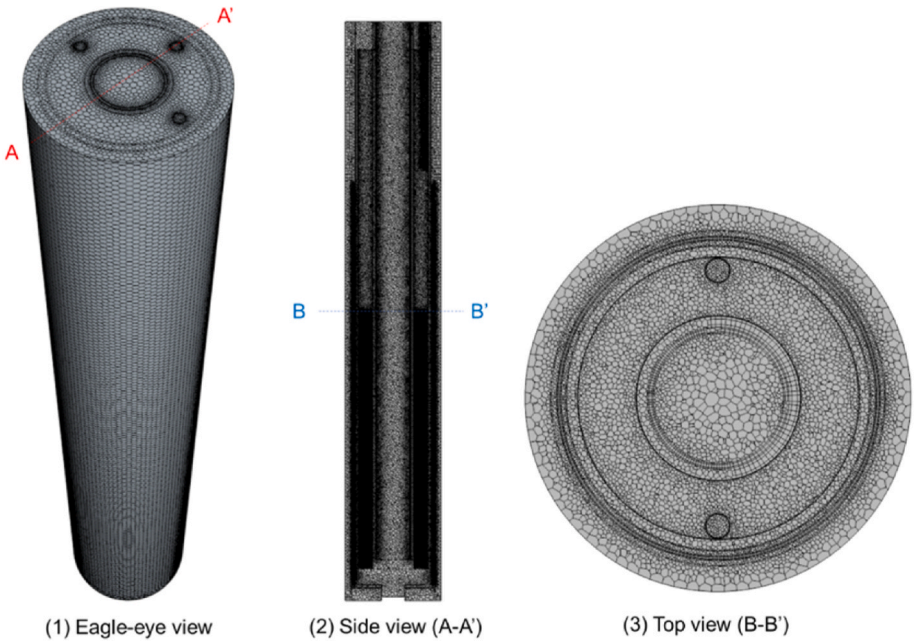

Fig. 10. Mesh structure of CFD model.

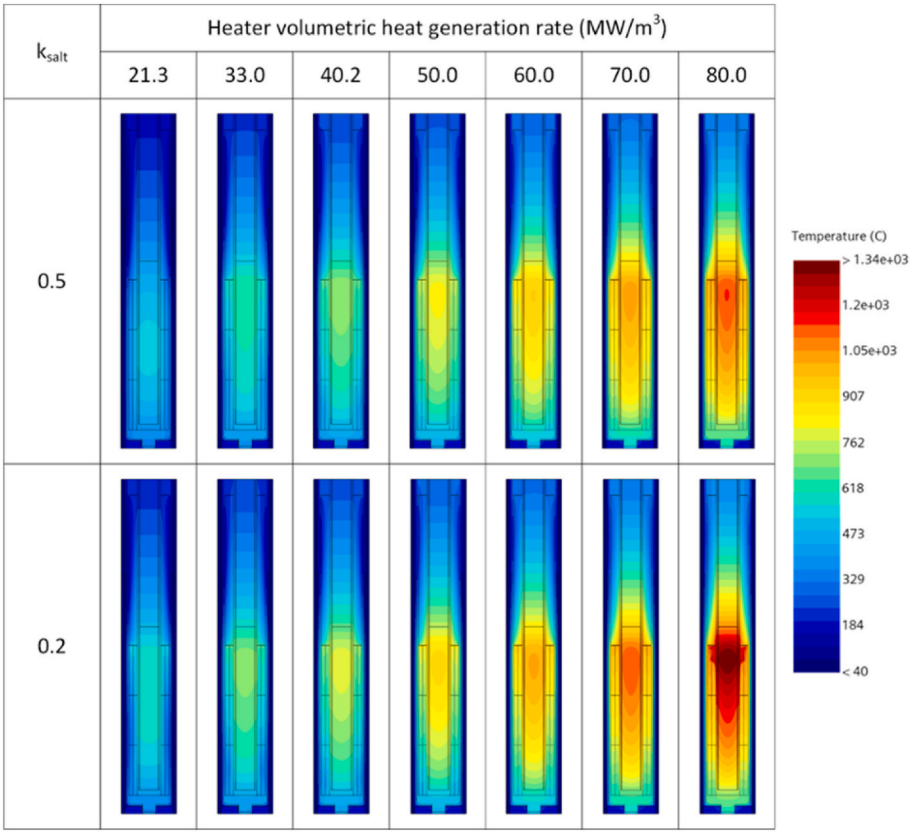

Fig. 11. Temperature distributions of MRTI device (no fission heating).

case, the calculated natural convection of the salt would be invalid. To examine the high-power condition, salt properties at high temperatures need to be provided.

Fig. 12 shows the minimum and maximum salt temperatures and the maximum heater temperature as a function of the heater heat generation rate. When the thermal conductivity of the salt decreased, the maximum temperatures of both the salt and heater thermowell increased. When a high salt thermal conductivity of 0.5 W/m-K was used, both the maximum temperature of the heater thermowell and the minimum temperature of the salt met the requirements with the heater heat generation rate between 60 MW/m^3 and 70 MW/m^3. When a low salt thermal conductivity of 0.2 W/m-K was used, the range of the heater heat generation rate resulted in temperatures that met the requirements for both salt and the structure became narrow. In this case, both the salt and the structure temperatures can meet the requirement when the heater heat generation rate is in the vicinity of 60 MW/m^3, which corresponds to a heater power of 252.45 W. It is deemed that the influence of the salt thermal conductivity on the minimum temperature of the salt was weak.

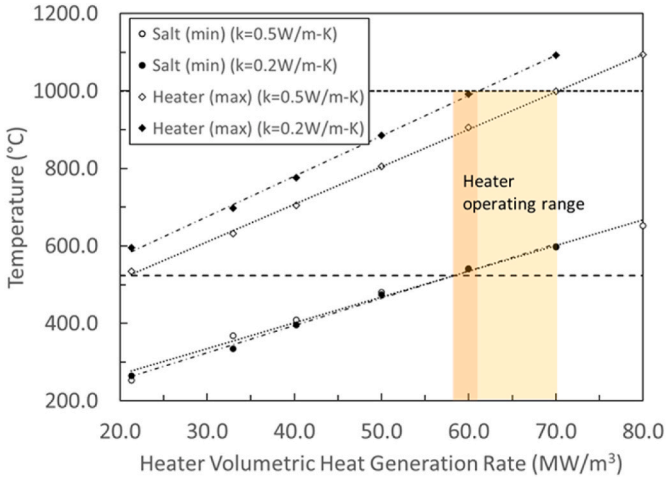

Fig. 12. Maximum temperature of heater thermowell and the minimum temperature of salt for various heater heat generation rates (no fission heating).

3.2.2. *CFD results for fission heating test*

The CFD calculation investigated the temperature distribution of the MRTI device with fission heating. Fig. 13 shows the temperature distribution of the MRTI device. The salt could be heated simultaneously by fission and the electric heater. For a high salt thermal conductivity of 0.5 W/m-K, above temperatures exceeded the valid range when the heater power was greater than 33.0 MW/m^3. The salt was heated more rapidly when the salt thermal conductivity was low. It was found that the natural convection of the salt was not appropriately simulated when the heater power was greater than 33.0 MW/m^3. However, for the heater volumetric heat generation rate less than 10 MW/m^3, the CFD results showed that the MRTI device will meet the temperature requirements of both structure and salt during the irradiation. During the irradiation test, the fission heating within the salt led to the upward flow at the middle of salt volume. As the heater power increased, the upward flow adjacent to the heater thermowell surface formed while the downward flow formed adjacent to the heater thermowell outer surface.

The maximum temperature of the heater thermowell and the minimum temperature of the salt with fission heating are illustrated in Fig. 14. In the CFD simulation with a low salt thermal conductivity of 0.2 W/m-K, the maximum temperature of the heater thermowell exceeded 1000 °C when the heater power was greater than 21.3 MW/m^3. However, the maximum temperature of the heater was lower than 1000 °C when the heater volumetric heat generation rate was less than 10 MW/m^3. The minimum temperature of the salt was higher than

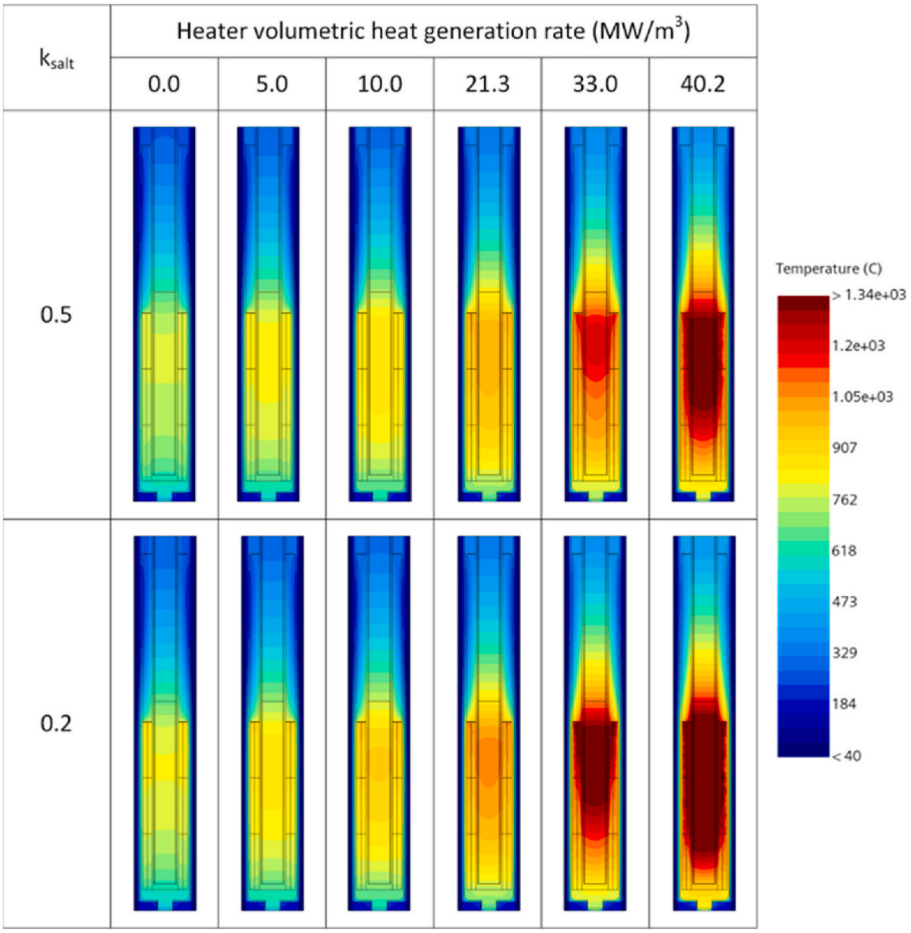

Fig. 13. Temperature distributions of MRTI device with fission heating.

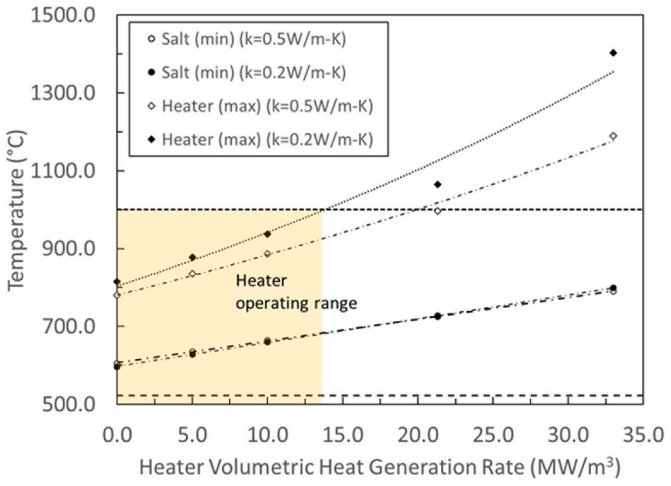

Fig. 14. Maximum temperature of heater thermowell and the minimum temperature of salt for various heater heat generation rates for various heater volumetric heat generation rates with fission heating.

523 °C regardless of the heater powers.

3.3. Stress calculations

The ability of the MRTI experiment capsule to fulfill its role as a safety-based containment structure was evaluated in two stages. First, the overall safety of the MRTI experiment was evaluated from an energy perspective. Second, analysis demonstrated reliable containment of all radioactive materials. The purpose was to demonstrate that the capsule material has the strength capacity to resist the expected stress from internal pressure. Design gaps were reviewed for thermal expansion issues that could initiate capsule failure.

The MRTI capsule is small and does not meet the typical definition of a pressure vessel. A common accepted pressure vessel definition is 'a closed vessel over 6-in (150-mm) diameter with a pressure difference greater than 15-psi (103.4 kPa)'. Consequently, the chosen design methodology satisfies standard engineering practices and not any specific consensus pressure vessel code.

The release of potential energy from a sudden rupture of a pressure vessel at maximum internal pressure has been used as a measure of the hazard to personnel and equipment for over two decades. A recognized safety threshold is 1000 lbf-ft (1350 J) of stored energy (Paulsen, 2009). The stored energy is historically calculated for gases or vapors above the boiling point by assuming isentropic expansion as per the equation:

$$W = \frac{P_1 V_1}{k-1}\left[1 - \left(\frac{P_2}{P_1}\right)^{\frac{(1-k)}{k}}\right]$$

Where W represents the work energy, k the ratio of specific heats, P_1 and P_2 the initial and 2nd state pressure respectively, and finally V_1, the initial volume. Initial conditions at capsule loading are ambient temperature 72 °F (22 °C), ambient pressure 12.5-psi (86.2 kPa), and gas volume 1.02-in^3 (16.65 cm^3). Adjusting for salt expansion and fission gas generation, final capsule conditions are temperature 1830 °F (1000 °C), internal pressure 71.5-psi (493 kPa), and gas volume 0.77-in^3 (12.57 cm^3). Solving for the final stored potential energy in the capsule

yields 4.5 lbf-ft (6.1 J). This is 220 times less than the recognized risk threshold of 1000 lbf-ft (1350 J). For additional comparison, an inflated 20-in diameter party balloon stores ~255 lbf-ft (345 J) or 56 times the energy. Clearly, a potential explosive rupture of a MRTI capsule is not a safety hazard for personnel or external equipment.

The capsule shell hoop stress was then calculated using standard formula with the final pressure listed above and additional inputs for cylinder diameter 0.776-in (19.7 mm), and shell thickness 0.0145-in (0.368 mm):

$$\sigma_h = \frac{P \times d}{2 \times t}$$

Where σ_h is the hoop stress, P the internal pressure, d the cylinder diameter, and t the shell thickness. The Inconel 625 shell material is estimated to have a yield strength of 14.2-ksi (98 MPa) at temperature. This is seven times the calculated hoop stress of 1.9-ksi (13.2 MPa) and documents the shell can reliably withstand the expected internal pressure.

A difference in expansion between the hot center heater well and the cooler capsule cylinder shell would lead to physical interference if an expansion gap was not provided. Thermal analysis in Fig. 15 shows temperature gradient is maximum in the lower capsule filled with salt and quickly diminishes above the salt (see Fig. 16).

The expansion difference was modeled by evaluating only the lower half of the capsule. The heater well seeing a temperature rise from ambient to 1830 °F (1000 °C) at a mean coefficient of expansion of 9.67 × 10^{-6}-in/in-F (17.4 × 10^{-6} m/m-C). The cylinder shell rising from ambient to 500 °C at a mean coefficient of expansion of 7.89 × 10^{-6}-in/in-F (14.2 × 10^{-6} m/m-C). The change in length was calculated per the formula:

$$\Delta l = \alpha_T \times l_i \times \Delta T$$

Where Δl is the length change, α_T the coefficient of expansion, l_i the initial length, and ΔT is the change in temperature. The calculated expansion differential was 0.029-in (0.74 mm). A design gap of 0.040-in (1 mm) was established between the heater well and the capsule end cap. This gap is sufficient to avoid destructive interference.

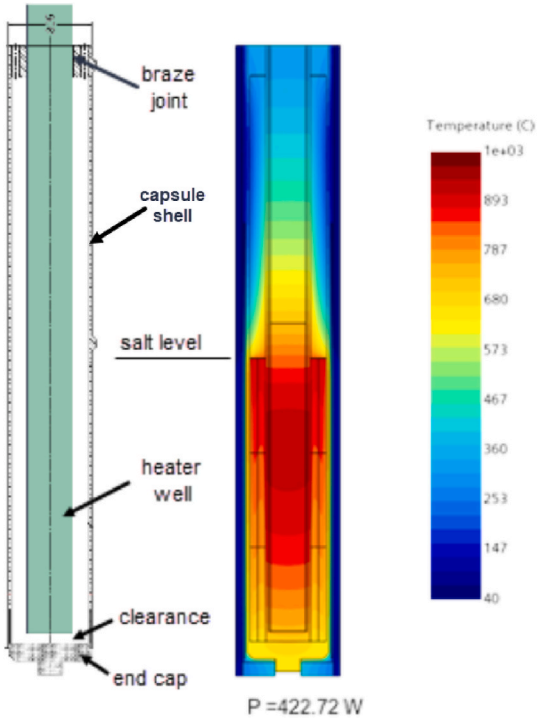

Fig. 15. Thermal gradient and expansion gap.

4. Experiment fabrication and testing

With the final design established and performance/safety criteria established, the project proceeded to the fabrication and testing of a prototype experiment to scale. The prototype assembly was filled with a non-fuel salt compound described in Table 6. The intent was to validate design and manufacturing assumptions without sensitive material. An out-of-pile setup that mimics the hydraulics conditions within the NRAD core was also developed in order to conduct a commissioning test for the prototype assembly.

4.1. Fabrication and assembly

Multiple fabrication and assembly techniques were required for the realization of the MRTI experiment vehicle. Firstly, sealing the capsule is critical to prevent fission gas and chloride off-gas release during experimentation and prior to PIE activities and thus, the results of the experiment. Two assembly steps are performed in order to seal the capsule system: (1) an induction braze of instrumentation and thermowell into the top of the capsule bulkhead; and (2) a laser weld of the bottom capsule cap.

To reduce the total number of leak paths and required welds a two-component capsule was investigated for manufacturability out of the IN625 material. The top capsule component was machined out of IN625 with the total height of the capsule and bulkhead penetrations machined for instrumentation and the bulkhead. Due to the high temperatures involved in the experiment, high temperature nickel braze materials were scoped for this assembly method. Between various braze materials, BNi-5 was chosen with a high melting point of ~1100 °C. Induction braze material processes are carefully developed in order to maximize material draw through the thickness of the penetration without damaging the base material or instrument. For high temperature braze materials such as BNi-5, with a melting point closer to the melting point of the base material, this can prove to be a challenge in the assembly process. Two INL braze procedures were developed and qualified via the American Society of Mechanical Engineers (ASME) Section IX standards for this braze. Three Type N thermocouples and the heater thermowell were qualified as an IN625 to IN625 bulkhead braze, while the pressure extension tube was qualified as a 300 series stainless steel to IN625 bulkhead braze. The preferred BNi-5 diametral gap was identified as approximately 0.001" (0.025 mm), and bulkhead penetrations were reamed to meet this fitment for each component. Each component was installed into the top capsule component at the desired depth through the bulkhead and placed under a flowing atmosphere of helium at a flowrate of 4 L/min. Ideal braze parameters result in a clear fillet on both the top and bottom of the instrument penetration and little-to-no signs of oxidation, cracks, or linear indications. The resulting brazed capsule components are shown in Fig. 16.

Various welding techniques were considered for the MRTI capsule assembly including Tungsten Inert Gas (TIG), autogenous TIG, and laser welding methods. The thin-walled geometry of the capsule and the need to avoid pre-melting of the salt by the welding process, the laser welding method was chosen with a high energy density on the weld joint. In

Table 6
Specification of the non-fuel salt used in the prototype.

Parameter	Value
Salt Compound	44 wt% LiCl - 66 wt% KCl[a]
Density	2.02 g/mL at 25 °C
Impurity levels	≤150.0 ppm
Melting point	357 °C

[a] From: https://www.sigmaaldrich.com/US/en/product/aldrich/479330.

Fig. 16. Braze development component with one IN625 instrument in an IN625 bulkhead (left), IN625 instruments and thermowell braze development piece (middle), in-process MRTI capsule brazing (right).

order to further protect the joint, an integral backer with an interference fit was designed for the interface between the capsule cap and the top capsule. This weld was design to be performed in glove box in an inert argon atmosphere. An INL weld procedure was developed for this bottom capsule cap weld and qualified via ASME Section IX standards. Development activities were focused on achieving the desired 100–150% penetration into the weld joint (full penetration, and up to 50% into the backer thickness), and minimal porosity. Fig. 17 shows an example of laser welding development components with good parameters. Porosity is ideally avoided, due to the low pressures involved in the experiment, weld join efficiency and joint strength is not of major concern. Certain volumetric inspections such as weld radiography will not be required for the assembly, however visual inspections for linear indications or cracks, and helium leak checks will ensure that the weld meets the operational requirements of the capsule.

Once the top capsule braze was completed for the non-fueled salt assembly, the pressure sensor or capped Swagelok union was installed onto the pressure extension tube and the top end of the capsule sealed. Following these steps, the non-fueled surrogate salt was loaded through the bottom of the capsule in a glovebox atmosphere. The surrogate salt used for this assembly was 99.99% purity anhydrous LiCl–KCl procured from Sigma-Aldrich and was sealed under argon in a glass ampoule by the manufacturer. Assembly of the non-fueled salt assembly was meant to reflect the required assembly steps for the eventual fueled salt assembly to imitate and practice these assembly steps. Custom capsule handling components were designed for in-glove box salt loading and capsule bottom installation. The capsule was installed in the designed clamp assembly to offset capsule from the glovebox floor and allow for space for coiled instrumentation to float. Once clamped into place, a custom stainless-steel funnel was used for salt fill into the capsule. For salt filling and glovebox assembly with the fuel salt, it is important to keep the atmosphere at less than 5 ppm O_2 and as low humidity as possible, and for the non-fueled salt assembly these limits were achieved. Intended salt weights were measured in-glove box, and then the weight of the filled capsule and funnel were taken after the filling process to confirm the mass of salt in the capsule. With the salt filled in the capsule the bottom cap was pressed onto the interference fit via a press jig designed into the capsule clamp assembly shown in Fig. 18. The assembly was then bagged in the argon glovebox atmosphere for transfer to the laser welding glovebox and the bottom cap weld was performed to seal the assembly. The capsule was helium leak checked with an acceptance criterion of no greater than 10^{-6} cc/sec leak rate (see Fig. 19).

Similar laser welds were used for the stainless-steel outer can containment with similar interference fit joints, qualification to ASME Section IX, and inspection acceptance criteria. Loading of the capsule and other components was performed on benchtop [as shown in Fig. 19]. The heater was installed in the capsule thermowell with a heat

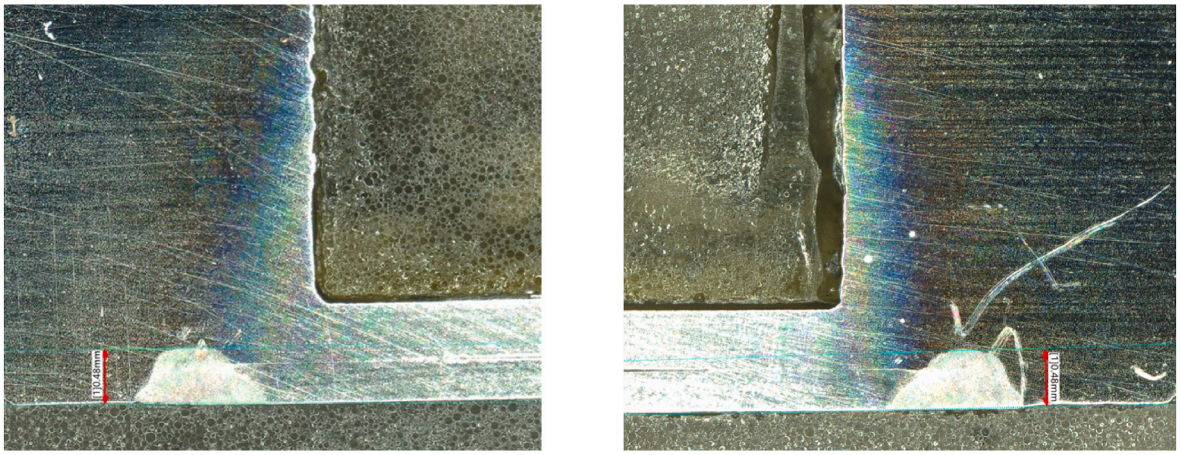

Fig. 17. Weld parameter development samples with good weld parameters.

Fig. 18. Brazed capsule top installed in clamp assembly (left), salt fill funnel (middle), and bottom cap press jig (right).

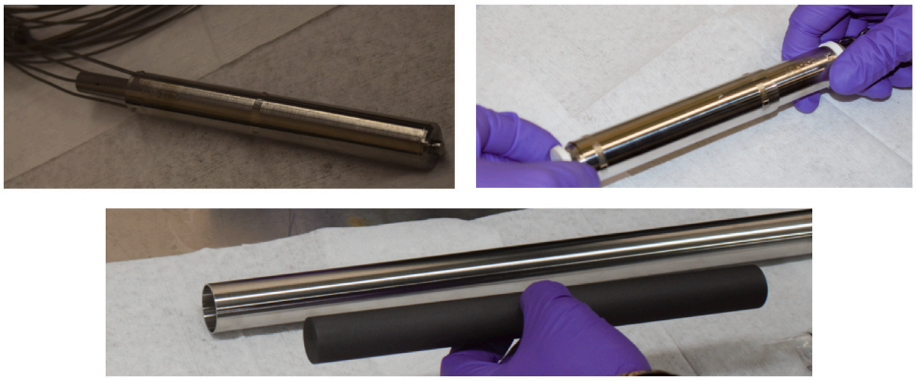

Fig. 19. Completed MRTI capsule (left), capsule assembled with insulative spacers and radiative heat shield (right), and graphite spacer (bottom).

transfer compound (T99 Thermon or similar) in order to ensure contact between the heater sheath and the thermowell inner diameter. Out-of-pile heater testing was performed in order to understand the heater performance and relative temperatures of the thermowell wall and internal heater TC prior to assembly the heater system. Additionally, before assembly, the individual heater was tested at temperature prior to installation in the thermowell with the heat transfer compound. For the outer can containment assembly, the first step was welding of the bottom outer can fitting to the outer can tube. The first item loaded afterwards was the graphite spacer. The capsule was pre-assembled with the bottom and top insulative spacers as well as the radiative heat shield. Instrumentation was routed around the pressure sensor and Swagelok fitting and the compression springs were slid over all instrumentation and placed onto the top insulation spacer. From this point the top, outer can fitting was slid over all instrumentation, all of the components were placed into the outer can containment tube, and the top fitting was pressed onto the top weld joint. The same procedure which welded the bottom fitting was then used to make the weld between the outer can containment tube and the top fitting. Portions of the outer can assembly process are pictured in Fig. 20.

In order to seal the instrumentation and ultimately seal the desired gas mixture in the gas gap of the capsule the Conax compression seal gland was installed on the top of the outer can top fitting. While in the glovebox with the intended gas mixture, the Grafoil seal and stainless steel followers were installed over all of the instrumentation, and the heater potting cut, and the Conax nut was torqued to manufacturers specifications. Upon this the glovebox atmosphere was sealed within the outer can containment, and the instrumentation was sealed out of the top of the assembly. Additions of epoxy on the Conax NPT fitting and on top of the Conax penetrations were considered for additional sealing for

Fig. 20. Assembly of MRTI capsule with compression springs and top fitting (top), and pressed and welded outer can containment assembly (bottom).

the assembly. Upon final inspections the MRTI non-fuel salt experiment assembly was complete and ready for commissioning testing. The final assembly is showcased in Fig. 21.

4.2. Commissioning test

Both mechanical assembly inspections and electrical system checks were performed to confirm functionality prior to initiating the commissioning test (see Fig. 21). Using the 1.5" (3.81 cm) outer can top fitting geometry the assembled MRTI prototype experiment was installed in the water jacket rig top flange assembly. The outer diameter of the outer can top fitting was sealed on the flange via a 1.5" (3.81 cm) Swagelok fitting with plastic ferrules. Three type K thermocouples were also sealed through the flange with Conax compression fittings and these thermocouples were attached to the MRTI outer can containment at desired axial positions. The purpose of these thermocouples was to record the outer can containment wall temperature at various axial positions during the commissioning test. The requirement is that the water at the outer containment does not exceed 70 °C. The experiment and flange were loaded and installed in the water jacket (Fig. 22). The cooling water flow was then connected and confirmed to be 0.2 gpm (see Fig. 23 for commissioning test setup below). This is expected to be representative of flow conditions within the NRAD core. Inlet and outlet temperatures of the jacket were also recorded via integrated thermocouples in the system.

Thermocouples and heater cabling were connected to the control system described in Section II(D). Temperature readings were checked via the user interface shown in Fig. 24. The system was heated to a series of set temperatures and held at each to ensure that the heater control system was capable of maintaining temperature within the salt capsule. Set temperatures of the test were: 350, 450, 550, 650, 750, and 850 °C. Above these temperature set points the system would be pushed to high temperature limits if possible. During the commissioning test, surrogate salt, components, and water temperatures remained within acceptable operating limits, even at elevated testing temperatures. This provided confidence that the design insulation (gas gap and radiative heat shield) was functioning properly for the temperature ranges of the system (see Fig. 25).

Control was established using thermocouple #206 (TC-206) which was a salt-immersed TC. During initial testing it was found that the integrated type K heater TC had high sensitivity to amperage sent through the heater, due to its close proximity to the heater coil wires in the core. Because of this the PID scheme used for this system was unable to hold a clear temperature increase rate between the setpoint, even with good PID tubing parameters. With the in-salt immersed TC, the system was able to hold a constant ramp rate and hold the temperature at the desired set point. However, the integrated heater TC was still utilized as the temperature shutoff limit for the system. The heater power was gradually increased and decreased via the PID controller to reach a range of targeted values between 350 °C and 750 °C as can be seen in Fig. 25.

Fig. 22. Loading of the MRTI prototype into the out-of-pile test rig.

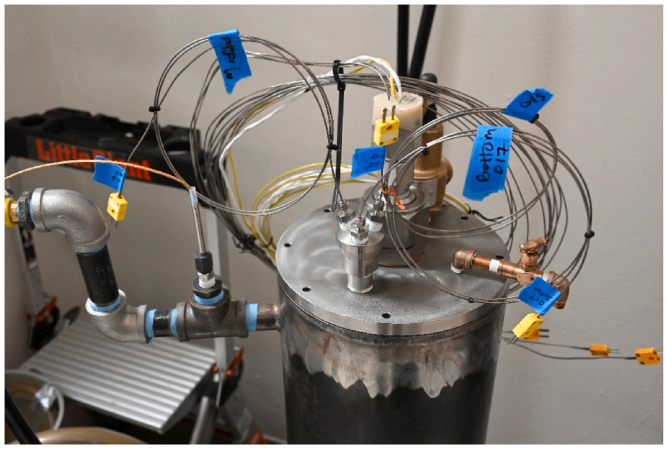

Fig. 23. Commissioning test setup with the salt capsule and outer can assembly inserted into the test rig prior to hookup and testing.

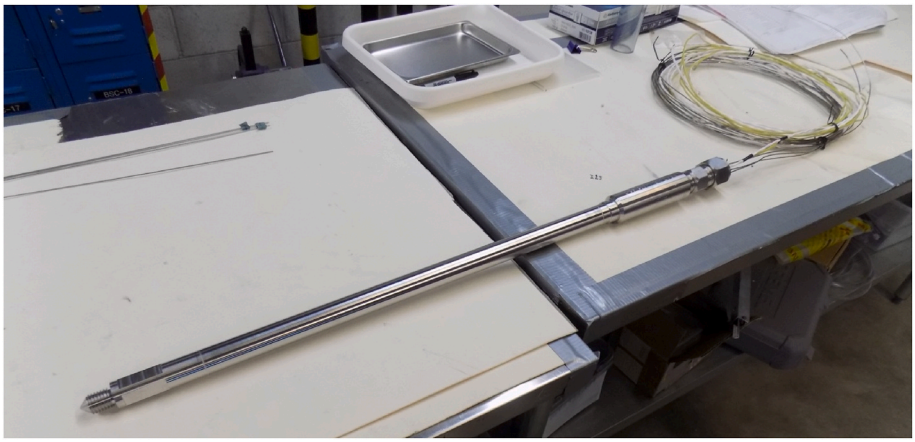

Fig. 21. Prototype final assembly (loaded with non-fuel salt).

Fig. 24. MRTI Programmable Logic Controller (PLC) interface for system control.

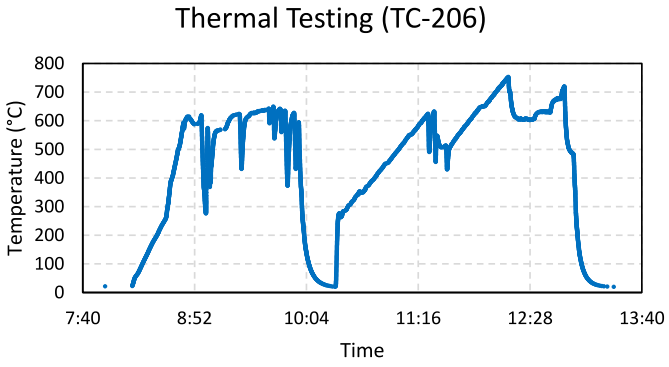

Fig. 25. Evolution of temperature readings at salt thermocouple #206 (TC-206) during the commissioning test.

System heater TC temperature limit errors caused a short shut off in the middle of the commissioning test, but with adjustments of the temperature shut off limit, the test was restarted. It is expected that cyclic testing of the system is also a noteworthy outcome. All the targeted temperature levels were reached with a maximum recorded temperature of 753 °C. Above this recorded temperature additional heater TC failures caused the over temperature limit to open circuit and it was concluded that, for this specific surrogate salt and heater defect, the maximum intended temperature would not be achievable.

The total elapsed testing time during this test period was about 5.5 h, during which, a heating rate of 7 °C/min was used. The outlet temperature of the water reached a maximum of 35 °C but was more consistently maintained at about 23 °C, which is well below the maximum allowable temperature of 70 °C for the NRAD reactor. The difference between the outlet and inlet temperatures was consistently approximately 4.5 °C, which is also below the target increase of less than 9 °C for intended NRAD operations. With the surrogate salt the system was able to hold the temperature without difficulty between the 550–650 °C range, well above the required melting temperature of the intended fuel salt temperature for the reactor experiment. Temperatures above the tested 750 °C are possible with design changes including better thermal contact between the heater sheath and the thermowell wall. With fission heat from the salt, it is expected that the heater will perform at very low amperage and just provide supplemental heat to the system during the bulk of the irradiation time. Overall, the commissioning test was deemed to be successful, and the design validated.

4.3. Preparations for post-irradiation examination

Upon irradiation, the irradiated experiment would be transferred to the main hot cell in the Hot Fuel Examination Facility (HFEF) via the cask tunnel located outside of NRAD's reactor room. The HFEF main cell would be the location where several PIE and PIE preparation activities take place. These activities would start with the examination of the integrity of the whole experiment. This would be followed by a confirmation of the disassembly strategy before proceeding to the dismantling of the outer can. Next, the fission product gamma signature would be examined. Gas samples from the plenum region would then be extracted, followed by the removal of salt from the capsule.

The extracted gas samples, removed irradiated salt samples, and the salt-facing material (inner capsule material) would be transferred to downstream PIE and characterization facilities (e.g., Analytical Research Laboratory [ARL], Molten Salt Thermophysical Examination Capability [MSTEC], and Irradiated Materials Characterization Laboratory [IMCL]) for isotopic composition of the gas plenum, examining the microstructure of the structural material, and measuring fuel salt properties (Fig. 26). The main PIE objectives will be to collect data on (1) source term characterization; (2) irradiation/fission product-induced corrosion; and (3) the evolution of thermophysical properties with fission product concentration.

For the purpose of focusing on the test vehicle, only certain PIE preparation activities in HFEF main hot cell are discussed in detail here.

4.3.1. Neutron radiography

The 250 kW NRAD is specifically used for large scale neutron radiography comparing to other neutron imaging facilities, where the beams are well collimated and moderated. NRAD has two neutron beamlines of higher content of epithermal to fast neutron energies, currently conducting neutron imaging for irradiated fuel specimens. The East Radiography Station (ERS) features the in-cell neutron radiography with the test vehicle lowered directly from the main cell floor. The North Radiography Station (NRS) houses an elevator shaft that allows specimens to be transferred into the shielded cell from a truck lock directly above. The MRTI experiment would utilize the ERS for integrity inspection as well as identifying disassembly strategy. Cadmium covered indium film (epithermal and above energy neutrons) would be used for highly enriched and large specimens, while the dysprosium film (thermal neutrons) would be used to reveal details.

4.3.2. Precision gross and isotopic gamma scanning (PGS)

The Precision Gamma Scanner (PGS) system consists of a sample stage in the main cell, a through-wall collimator, and an ultra-low background high purity germanium (HPGe) detector with Compton background suppression outside of the hot cell. The PGS system uses various apertures to create a small slit of various sizes to allow characteristic gamma rays from various fission products to reach the detector. Upon disassembling the outer capsule, the MRTI experiment would be transferred to the sample stage, which can move along the x, y, and z axes as well as rotate freely. These features would allow the PGS to provide cross-sectional and three-dimensional distribution of individual isotopes.

4.3.3. Gas Assay, Sample and Recharge (GASR) system

The salt containing inner capsule would be transferred to the Gas Assay, Sample and Recharge (GASR) system for gas extraction. The GASR system uses a Nd-YAG pulsed laser with peak power at 1500 W and average power of 150 W to puncture the inner capsule at the gas plenum location identified by neutron radiography. Then the gas sample would be extracted by the mechanical vacuum through the through-wall channel. The GASR system can also determine the void volume and gas pressure by monitoring the backfill gas. The extracted gas samples

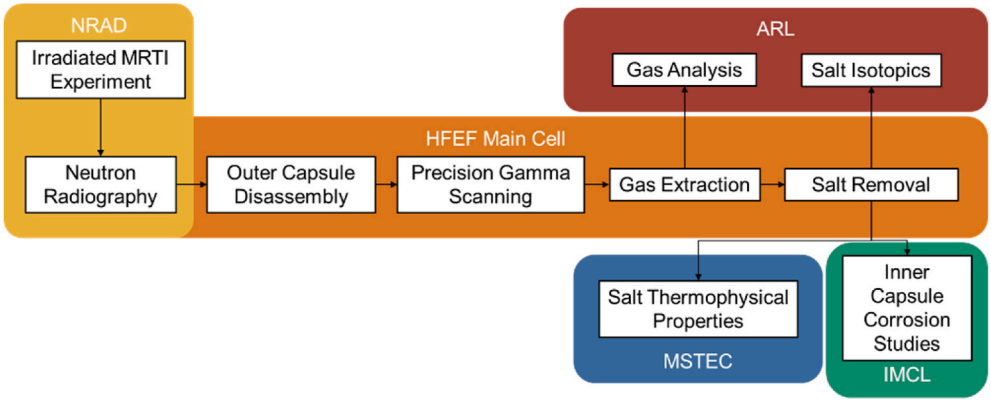

Fig. 26. MRTI PIE Plan flowchart.

would be transferred to ARL for gas analysis.

In order to accommodate the laser penetration power and to form a good seal for successful gas extraction, MRTI experiment's inner capsule was redesigned to have an outer diameter of 0.805″ to interface the GASR seal assembly (Fig. 27) and reduce Inconel 625 wall thickness from 0.079″ to 0.029″.

4.3.4. salt removal experiment in preparation for PIE activities

Salt removal experiments were conducted for various inner capsule geometries. The findings were first reported in (Abou-Jaoude et al., 2021c). While thinner annuli resulted in lower salt ΔT, capillary forces may complicate their removals during PIE. To assess this, salt removal prototyping experiments were conducted. Three capsule variations were manufactured with salt annuluses of 0.3, 0.4 and 0.5 cm thick. A surrogate salt of LiCl–KCl eutectic was taken to be representative. Wires and steel rods were placed inside each capsule to mimic the potential thermal and mechanical impact of sensors and thermowells. After the salt in powder form was inserted, the capsules were placed in a 500 °C heater as shown in Fig. 28. The salt was then left to solidify overnight (see Fig. 29).

Using an electric impact driver in a positive pressure glove box, the capsules were mounted and continuously vibrated to break up and remove the salt. By first removing the thermowell surrogate rod during the process, the salt could more easily extracted. Recovery of up to 99.2% of salt mass were reached as shown in Table 7. It is worth noting that variations in removal rates were primarily due to experimental setup rather than annulus thickness itself.

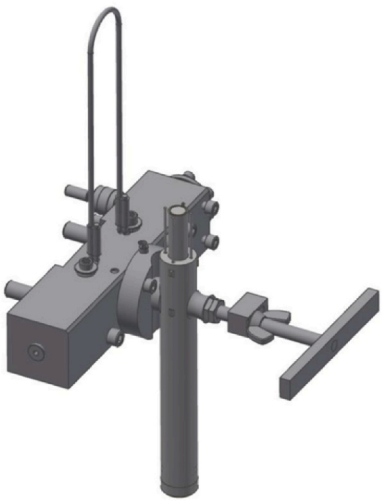

Fig. 27. 3D rendering of the MRTI inner capsule and GASR seal interface.

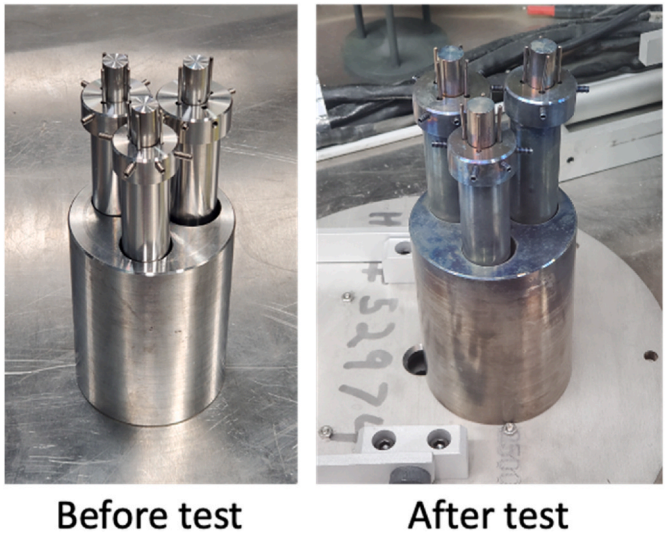

Fig. 28. Salt removal mockup test before/after insertion into heater. Taken from (Abou-Jaoude et al., 2021c).

After the salt removal, the salt samples would be transferred to MSTEC for thermophysical property measurements and to ARL for isotopic analysis. The inner capsule would be dissected into small samples to be used for corrosion studies in IMCL.

5. Conclusions

The paper details the design and engineering activities alongside the testing conducted to de-risk the demonstration of an enriched fuel salt irradiation capability. This is an experimental capability that is expected to be critical to future deployment of MSR designs. Irradiation tests are time-consuming, expensive campaigns that necessitate extensive planning and testing activities to increase the probability of experimental success—success in this case is defined as an acceptable amount of irradiated salt under a controlled temperature. Towards this end goal, several key steps including simulation, salt synthesis, assembly, PIE preparations, and full-scale prototyping activities were all conducted prior to assembling the final test device. The results of these activities yielded the desired outcomes: the design, when built, can reach adequate temperature distribution per the design requirements, both when the reactor is turned off and on. The salt can be synthesized and removed from the capsule following irradiation. Lastly, it was shown that in a prototypic flowing water environment, both programmatic and safety requirements can be met. The results conclude that t he project has established the foundation for a future in-pile irradiation capability

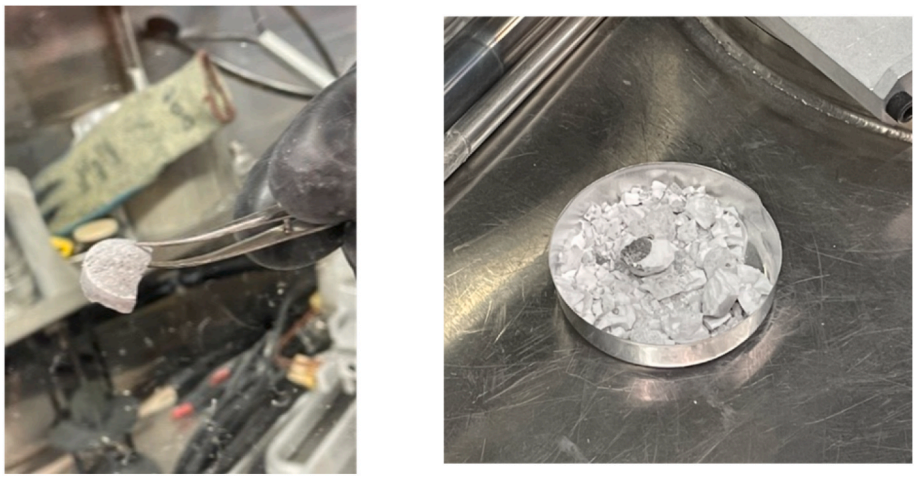

(a) (b)

Fig. 29. Extracted salt following prototype testing. Taken from (Abou-Jaoude et al., 2021c).

Table 7
Salt removal rate after melting/freezing.

Annulus Thickness	Initial Salt Mass	Recovered Salt Mass	Recovered Fraction
0.3 cm	15.000 g	13.892 g	0.926
0.4 cm	20.001 g	15.908 g	0.795
0.5 cm	25.002 g	24.804 g	0.992

for molten salts.

The project team will now move towards assembling the final test device, loaded with enriched uranium salt, to obtain irradiated salt for post-irradiation examination activities. These activities will unlock the scientific outcomes of the project.

Declaration of competing interest

The authors declare that they have no known competing financial interests or personal relationships that could have appeared to influence the work reported in this paper.

Data availability

Data will be made available on request.

Acknowledgement

This paper was authored by Battelle Energy Alliance LLC at Idaho National Laboratory under contract no. DE-AC07-05ID14517 with the Department of Energy. This research work was funded through the INL Laboratory Directed Research and Development (LDRD) program, grant number 21A1050-016FP, under the Department of Energy (DOE) Idaho Operations Office.

The United States Government retains, and by accepting the article for publication, the publisher acknowledges that the United States Government retains, a non-exclusive, paid-up, irrevocable, worldwide license to publish or reproduce the published form of this work, or allow others to do so, for United States Government purposes.

The authors gratefully acknowledge the contribution of the various other colleagues as part of the design and fabrication effort, namely Matilda Lindell, Stacey Wilson, Changhu Xing, and Connor Michelic.

References

Abou-Jaoude, A., Palmer, J., Sterbentz, J., Calderoni, P., 2019. Evaluation of a Versatile Experimental Salt Irradiation Loop (VESIL) inside the Advanced Test Reactor. Idaho National Laboratory, Idaho Falls. INL/EXT-19-52917.

Abou-Jaoude, A., Walker, S., Bhaskar, S., Ji, W., 2020. Feasibility assessment of a natural-circulation salt irradiation loop in the advanced test reactor. Nucl. Technol. 207 (12), 1821–1841.

Abou-Jaoude, A., Walker, S., Bhaskar, S., Jei, W., 2021a. Feasibility assessment of a natural-circulation salt irradiation loop in the advanced test reactor. Nucl. Technol. 207 (12), 1821–1841.

Abou-Jaoude, A., Chandler, J., Core, G., Davies, K., Downey, C., Phillips, W., Tan, C., Wilson, S., 2021b. Conceptual design of a temperature-controlled fueled-salt irradiation experiment to support advanced nuclear reactors. In: International Mechanical Engineering Congress and Exposition. Virtual.

Abou-Jaoude, A., Downey, C., Core, G., Davies, K., Phillips, W., Tan, C., Yoon, S., Wilson, S., 2021c. Design and Protoyping of a Fissile-Bearing Chloride Salt Irradiation Experiment. Transaction of the American Nuclear Society. Virtual.

Altahhan, M., al, e., 2019. 3D coupled transient simulation of a fast liquid fuel molten salt reactor primary loop using GeN-foam. In: NURETH, p. 18. Portland, OR.

AREMCO, 2023. Aremco AREMCOLOX™ 502-1400 (Bisque-Fired) Machinable Alumina, 1 1 [Online]. Available: http://www.matweb.com/search/datasheettext.aspx?matguid=501f3c56cb744d2cbade5ed7615032a1.

ASM International, 1990. ASM Handbook Volume 1, Properties and Selection: Irons, Steels, and High-Peformance Alloys.

Bess, J.D., Higgs, J.B., Lell, R.M., 2014. Neutron Radiography (NRAD) Reactor 64-Element Core Upgrade. Idaho National Laboratory, Idaho Falls, ID. INL/EXT-13-29628.

Cottrell, W., Hungerford, E., Leslie, J., Meem, J., 1955. Operation of the Aircraft Reactor Experiment. Oak Ridge National Laboratory. ORNL-1845.

Desyatnik, V.N., Katyshev, S.F., Raspopin, S.P., Chervinskii, Y.F., 1975. Density, surface tension, and viscosity of uranium trichloride-sodium chloride melts. Sov. Atom. Energy 39, 649–651.

Ezell, N.D., Raiman, S., Kurley, J.M., McDuffee, J., 2021. Neutron irradiation of alloy N and 316L stainless steel in contact with a molten chloride salt. Nucl. Eng. Technol. 53 (3), 920–926.

Farmer, M., Weathered, M., Lisowski, D., Bremer, N., Kilsdonk, D., Stack, T., Tomlin, C., Plucker, C., Moreno, E., Kong, R., Quan, Z., Dix, A., Kim, S., Ishii, M., Anderson, M., Napora, A., 2022. Development of a sodium fast reactor cartridge loop testing capability for the versatile test reactor. Nucl. Sci. Eng. 196 (1), 148–164.

Forsberg, C.W., Peterson, P.F., Sridharan, K., Hu, L., Fratoni, M., Kant-Prinja, A., 2018. Integrated FHR Technology development: trititum management. Materials Testing, Salt Chemistry Control, Thermal Hydraulics and Neutronics, Associated Benchmarking and Commercial Basis. NEUP Report, MIT-ANP-TR-180.

GmbH, M.W., 2023, 1 1. https://woite-edelstahl.com/alloy800en.html.

Hania, P.R., 2018. MSR irradiation program at NRG petten. In: MSR Workshop 2018. Oak Ridge.

Idaho National Laboratory. 250 kW TRIGA neutron radiography reactor. https://mfc.inl.gov/SitePages/Instruments/Hot%20Fuel%20Examination%20Facility/250%20kW%20TRIGA%20Neutron%20Radiography%20Reactor.aspx. (Accessed 3 March 2023).

Kieruj, P., Prezestaki, D., Chwalczuk, T., 2016. Determination of emissivity coefficient of heat-resistant super alloys and cemented carbide. Archives of Mechanical Technology and Materials 36 (1), 30–34.

McDuffee, J., Christensen, R., Eichel, D., Simpson, M., Phongikaroon, S., Sun, X., Baird, J., Burak, A., Chapel, S., Choi, J., Gorton, J., Killinger, D.H.D., Miller, S.,

Palmer, J., Petrie, C., Sweeney, D., Schrell, A., Vollmer, J., 2022. Design and control of a fueled molten salt cartridge experiment for the versatile test reactor. Nucl. Sci. Eng. 196 (1), 234–259.
Mourogov, A., Bokov, P.M., 2006. Potentialities of the fast spectrum molten salt reactor concept: REBUS-3700. Energy Convers. Manag. 47 (17), 2761–2771.
NIST Chemistry Webbook, 2023. NIST Chemistry Webbook. January, p. 1. https://webbook.nist.gov/cgi/fluid.cgi?P=1&TLow=40&THigh=1490&TInc=25&Digits=5&ID=C7440371&Action=Load&Type=IsoBar&TUnit=C&PUnit=atm&DUnit=kg%2Fm3&HUnit=kJ%2Fkg&WUnit=m%2Fs&VisUnit=Pa*s&STUnit=N%2Fm&RefState=DEF.
Paulsen, S., 2009. Pressure Systems Stored-Energy Threshold Risk Analysis. Pacific Northwest National Laboratory, Richland, Washington. PNNL-18696.
Pelowitz, D.B., Goorley, J.T., James, M.R., Booth, T.E., Brown, F.B., Bull, J.S., Cox, L.J., , J. W. D. Jr., Elson, J.S., Fensin, M.L., , R. A. F. III, Hendricks, J.S., , H. G. H. III, Johns, R.C., Kiedrowski, B.C., Martz, R.L., Mashnik, S.G., 2013. MCNP6 User's Manual v1.0. Los Alamos National Laboratory. LA-CP-13-00634.
Savage, H.C., Campere, E., Baker, J.M., Bohlmann, E.G., 1960. Operation of Molten-Salt Convection Loops in the ORR. Oak Ridge Naitonal Laboratory.
Se, S., Y, S., Bang, I., 2016. Review on the current status of molten chloride reactor and its future prospects. In: Transactions of the Korean Nuclear Society Automn Meeting. Gyeongju, Korea.
Silfka, A.J., Filla, B.J., Phelps, J.M., 1998. Thermal conductivity of magnesium oxide from absolute, steady-state measurements. Journal of Research of the National Institute of Standards and Technology 103 (4), 357–363.
Special Metals, 2023, 1 1. https://www.specialmetals.com/documents/technical-bulletins/inconel/inconel-alloy-625.pdf.
Thoma, R.E., 1971. Chemical Aspects of MSRE Operations. Oak Ridge National Laboratory. ORNL-4658.
Trauger, D.B., Colin, J.A., 1961. Circulating fused-salt fuel irradiation test loop. Nucl. Sci. Eng. 9, 346–356.